Published in final edited form as:

Cell Rep. 2019 April 09; 27(2): 514–524.e5. doi:10.1016/j.celrep.2019.03.030.

Obesity Expands a Distinct Population of T Cells in Adipose Tissue and Increases Vulnerability to Infection

Ichiro Misumi[1], **Joshua Starmer**[1], **Toru Uchimura**[1], **Melinda A. Beck**[2], **Terry Magnuson**[1], **Jason K. Whitmire**[1,3,4,*]

[1]Department of Genetics, UNC-Chapel Hill School of Medicine, Chapel Hill, NC, USA

[2]Department of Nutrition, UNC-Chapel Hill Gillings School of Global Public Health, Chapel Hill, NC, USA

[3]Department of Microbiology & Immunology, UNC-Chapel Hill School of Medicine, Chapel Hill, NC, USA

SUMMARY

Obesity in humans is associated with poorer health outcomes after infections compared with non-obese individuals. Here, we examined the effects of white adipose tissue and obesity on T cell responses to viral infection in mice. We show that lymphocytic choriomeningitis virus (LCMV) grows to high titer in adipose tissue. Virus-specific T cells enter the adipose tissue to resolve infection but then remain as a memory population distinct from memory T cells in lymphoid tissues. Memory T cells in adipose tissue are abundant in lean mice, and diet-induced obesity further increases memory T cell number in adipose tissue and spleen. Upon re-challenge infection, memory T cells rapidly cause severe pathogenesis, leading to increases in lipase levels, calcification of adipose tissue, pancreatitis, and reduced survival in obese mice but not lean mice. Thus, obesity leads to a unique form of viral pathogenesis involving memory T cell-dependent adipocyte destruction and damage to other tissues.

Graphical Abstract

*Correspondence: jwhitmir@email.unc.edu.

[4]Lead Contact

AUTHOR CONTRIBUTIONS

I.M. and J.K.W. designed all studies and wrote the manuscript. I.M. performed all mouse experiments, including cellular immunology, FACS sorting of cells, virus quantification, physical health measures, and histological analyses at necropsy. T.U. assisted with the flow cytometry studies. J.S. and T.M. contributed to the statistical analyses of RNA-seq data. M.A.B. provided valuable guidance related to the design and interpretation of experiments related to obesity.

SUPPLEMENTAL INFORMATION

Supplemental Information can be found online at https://doi.org/10.1016/j.celrep.2019.03.030.

DECLARATION OF INTERESTS

The authors declare no competing interests.

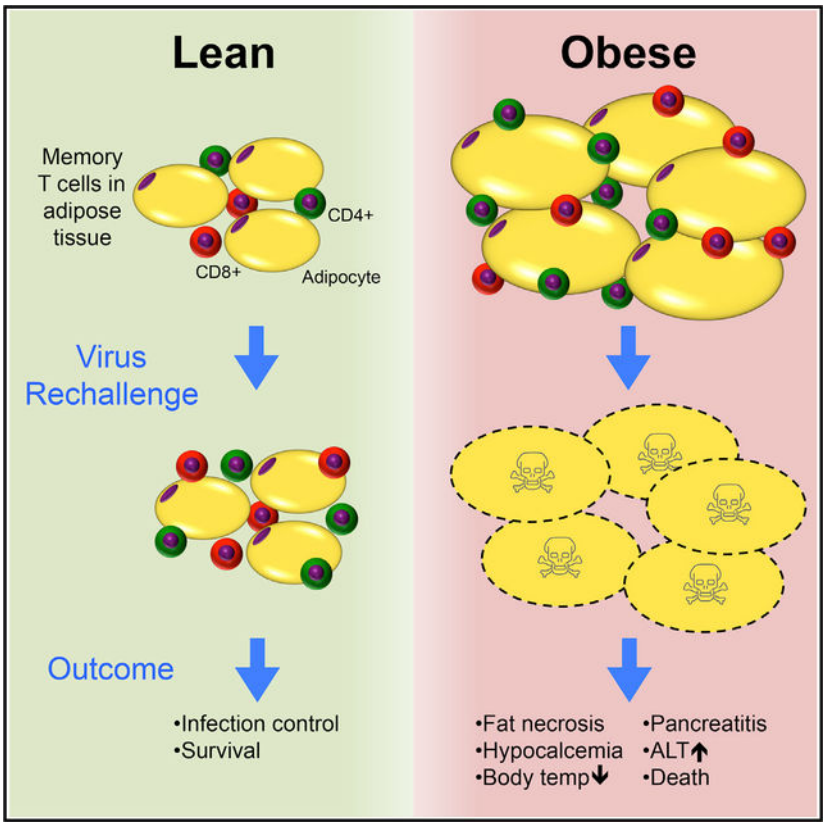

In Brief

Obesity is associated with increased morbidity and mortality after viral infections. Using a mouse model of obesity, Misumi et al. identify a distinct population of memory T cells in white adipose tissue and a memory cell-dependent pathogenic response to infection that leads to acute fat necrosis, pancreatitis, and lethality.

INTRODUCTION

Obesity is associated with impaired immune responses to viral and bacterial infections and an increase in the frequency of nosocomial infections compared with non-obese patients (Díaz et al., 2011; Huttunen and Syrjänen, 2013; Milner and Beck, 2012; Tsatsanis et al., 2010; Twig et al., 2018). Obese subjects also show a greater decline in influenza-specific antibody and CD8+ T cells after vaccination compared with non-obese subjects (Sheridan et al., 2012). These effects are replicated in mouse models of influenza infection, in which diet-induced obesity impairs memory T cell responses after vaccination and increases mortality following challenge infection (Karlsson et al., 2010; Smith et al., 2007). Obesity can alter other aspects of host responses to infection, such as prolonging inflammation and impairing wound repair following influenza infection (O'Brien et al., 2012) and worsening the progression of HCV-induced liver disease. Obesity-associated inflammation may contribute to co morbidities associated with obesity, including increased incidence of acute pancreatitis, cardiovascular disease, diabetes, and cancer, each of which has an underlying immune

component. Because obesity is increasingly prevalent, it is important to understand how obesity affects host defenses against different infections.

Obesity involves an increase in the mass of white adipose tissue (WAT), a physiologically significant tissue that regulates metabolism and nutritional homeostasis (Rosen and Spiegelman, 2014). WAT consists of adipocytes, endothelial cells, fibro-blasts, and immune cells, which change in abundance and function during the course of obesity. Obesity-induced changes in WAT include alterations in adipokine production, increased expression of pro-inflammatory cytokines, and the accumulation of M1 macrophages. However, it is unclear how these changes within adipose tissue may alter systemic adaptive immune responses to infection.

To understand the impact of WAT and obesity on T cell-based defenses, we examined the effect of obesity on memory T cell number and function in mice given acute lymphocytic choriomeningitis virus (LCMV-Armstrong) infection, a natural pathogen of mice that induces well-defined inflammatory, T cell, and B cell responses. We show that LCMV replicates in the WAT, resulting in virus-specific T cells that infiltrate the tissue, eliminate the infection, and persist there as memory cells. Memory T cells in WAT express unique phenotypic markers compared with memory T cells in the spleen. Adipose tissue T cells represent a major fraction of virus-specific T cells in mice, a population that was increased numerically by diet-induced obesity. Upon re-challenge with a disseminating variant of LCMV, immune obese mice, but not immune lean mice, showed greatly increased mortality that was T cell dependent and associated with fat necrosis, systemic release of lipases, and pancreatitis. Our data reveal a subset of memory cells that are greatly increased by obesity and associated with pancreatitis during infection.

RESULTS

LCMV Replicates in WAT and Is Resolved by 2 Weeks

As an initial approach to understanding the contribution of the adipose tissue to local and systemic immune defenses, the level of infection within the perigonadal WAT was quantified at multiple times after LCMV-Armstrong infection. At day 4, the adipose tissue was highly infected, although there was about 100-fold less virus per gram than in the spleen (Figure 1A). The adipose tissue continued to have high amounts of infection (10^5 plaque-forming units [PFUs]/g) at day 8, whereas the infection was reduced to the limits of detection in the spleen. LCMV was cleared in both tissues by day 12, and there was no recrudescence at later times (Figure 1A and data not shown). The kinetics and magnitude of infection differed in the spleen and WAT, which may relate to the availability of permissive targets in each site or the speed with which T cells can reach the tissue.

Adipocytes have a unique appearance; they are typically large with a lipid droplet, minimal cytoplasm, and a nucleus that is often adjacent to the plasma membrane. Gentle, differential centrifugation was used to separate adipocytes from cells of the stromal vascular fraction (SVF), a cell population that includes leukocytes, mesodermal or mesenchymal stromal vascular cells, pre-adipocytes, adipose-derived stem cells, pericytes, endothelial cells, and fibroblasts (Figure 1B). Although most virus was recovered in the stromal vascular fraction,

adipocytes carried low levels of infectious virus, roughly one-tenth the amount present in the entire tissue. Thus, WAT and adipocytes themselves are associated with viral infection.

LCMV infection resulted in inflammation of the WAT (Figure 1C, top). Areas of inflammation contained leukocytes, and the adipocytes within these foci were smaller in size than neighboring adipocytes, suggesting apoptosis (Cinti et al., 2005). Immunofluorescence staining revealed an increased population of CD3+ cells in the adipose tissue at days 14 and 40 after LCMV (Figure 1C, bottom). Compared with adipose from uninfected mice, there was a 10-fold increase in leukocytes recovered from the WAT at day 8 (Figure 1D). Much of this increase was due to a 280-fold increase in CD8+ T cells, resulting in ~ 4×10^6 CD8+ T cells in the perigonadal adipose tissue. There was also a significant 6.7-fold increase in CD4+ T cells, leading to ~ 2×10^5 CD4+ T cells in the WAT at day 8. CD4+ T cells continued to increase to >20-fold by day 12, resulting in a peak of ~ 10^6 CD4+ T cells (Figures 1D and S1C). During the first 2 weeks following infection, the relative increase in T cell frequencies was far greater in the WAT than in the spleen (Figures S1A–S1C). This was especially apparent when analyzing activated CD8+CD44^{hi} and CD4+CD44^{hi} T cells at day 8 (Figure S1D), which are likely specific for various epitopes of LCMV (Masopust et al., 2007). An inflated population of CD8+CD44^{hi} and CD4+CD44^{hi} cells remained in the WAT to day 70 (Figure S1D). Thus, infection in WAT is associated with an early accumulation of T cells, virus elimination, and then persistence of a pool of CD44^{hi} T cells.

A Distinct Pool of Virus-Specific T Cells Accumulates in WAT after Infection

Virus-infected cells should be recognizable by CD8+ T cells because MHC-I is expressed on adipocytes and infiltrating leukocytes. MHC-II is expressed by infiltrating F4/80+ macrophages but can be induced on adipocytes (Deng et al., 2013; Huh et al., 2014), so virus-specific CD4+ T cells may recognize viral material presented by antigen-presenting cells or possibly infected adipocytes. Because the infection was controlled in the adipose tissue and there was histological and fluorescence-activated cell sorting (FACS)-based evidence of infiltrating T cells, we considered that virus-specific T cells entered the tissue and mediated immune control.

Virus-specific T cells in the adipose tissue and spleen were quantified by tetramers at different times after infection. There was a prominent increase in the frequency of tetramer+ T cells in the WAT after infection, with the highest percentages at 1–2 weeks post-infection (Figures 2A and 2B). $GP_{33–41}$-specific CD8+ T cells in the WAT peaked in abundance at day 8 and were roughly 30-fold less abundant than in the spleen (Figure 2B). Major expansions were also seen for $DbNP_{396–404}$-specific and $DbGP_{276–286}$-specific CD8+ T cells after infection (Figure S1E). The I-$A^bGP_{67–80}$-specific CD4+ T cell response in the spleen peaked at day 8 (Figures 2A and 2B), whereas the CD4+ T cell response in the WAT peaked at day 13 and was roughly one-third that in the spleen at this time (Figure 2B). Thus, during the first 2 weeks of infection, as many as 5×10^5 D^bGP_{33}-specific CD8+ T cells and 1×10^5 IA^bGP_{67}-specific CD4+ T cells were in the fat pads. For perspective, these cells represented roughly 10% of what was present in the spleens of the same mice. In summary, the WAT represents a major site of virus-specific T cells that is largely uncharacterized.

After the peak response, there was a proportional ~ 10-fold contraction in $DbGP_{33}$+ CD8+ T cells in both tissues by day 24 that stabilized in the spleen but continued to decline in the WAT before reaching stability at day 70 at roughly 10^4 cells (Figures 2A and 2B). Approximately 10^4 $DbNP_{396–404}$-specific and $DbGP_{276–286}$-specific CD8+ T cells were also found in WAT at memory time points (Figure S1E). Similar to the CD8+ T cell response, IA^bGP_{67}-specific CD4+ T cells were relatively stable in the spleen from day 24 onward, whereas tetramer+ CD4+ T cells continued to decline in the WAT between days 24 and 70. Thus, the CD4+ T cell response in WAT shows a delayed expansion and appears less stable compared with the spleen. At day 70 and 90 post-infection, memory CD4+ T cells in adipose tissue were roughly 5% of the number found in the spleen (Figure 2B and data not shown).

The capacity of memory T cells to respond to antigen was assessed by intracellular cytokine staining (ICCS) assay. There was a large increase in the percentage of CD8+ T cells that could make IFNg (or TNF or IL-2) in response to $GP_{33–41}$, $NP_{396–404}$,or $GP_{276–286}$ peptides in the spleen and WAT (Figures 2C–2E and S1F and data not shown), and these cells underwent contraction and were maintained to days 30–70. The overall number of cytokine-expressing memory CD8+ T cells was smaller in WAT compared with spleen (Figures 2C, 2D, and S1F). Memory GP_{33}-specific CD8+ T cells in the spleen made >2-fold more IFNg per cell than those in the WAT (Figure S1G), perhaps because adipose tissue CD8+ T cells express PD1 (Figure S1H) and may be inhibited. The frequency of memory CD4+ T cells that could make IFNg in response to $GP_{61–80}$ was greater in the WAT than spleen (Figure 2C), though the overall number of cytokine-expressing memory CD4+ cells was lower in the WAT compared with spleen (Figures 2D and S1F). The amount of cytokine made per CD4+ T cell in each compartment was similar (Figure S1G). These data show that the memory T cells persisting in WAT are capable of making pro-inflamma-tory cytokines.

Nearly all T cells in the spleen and WATwere Ki67+at day 8, indicating that the cells were actively dividing in response to infection (Figure S1I). For virus-specific CD8+ T cells, cell division quickly subsided to background levels (~10%) in both compartments by day 13, although a low level of staining (<20%) could be observed for splenic GP_{276}-specific CD8+ T cells at day 21. In contrast, 60% of CD4+ T cells continued to proliferate at day 13 before subsiding to levels near background by day 21. In contrast to GP_{33}-specific CD8+ T cells, GP_{61}-specific CD4+ T cells incorporated BrdU when mice were pulsed from day 13 to 20 or from day 21 to 28 (Figure S1J). Interestingly, CD4+ T cells in the WAT showed far more BrdU incorporation than those in the spleen, suggesting that the adipose tissue environment sustains the proliferation of subsets of antigen-specific T cells for 2–3 weeks after infection has resolved. The percentage of CD4+ T cells incorporating BrdU appeared to decline over time, suggesting that factors in adipose tissue that stimulate CD4+ T cell proliferation diminish through this period, and normal homeo-static mechanisms may be at play at later memory time points.

Memory T Cells Present in WAT Are Distinct from Lymphoid, Circulating, and Mucosal Subsets

Subsets of tissue-resident memory T (Trm) cells can be found in lung, skin, or intestinal locations following vaccination or infection. Trm cells are distinct from T cells circulating within the vascular system and persist locally in specific tissue sites for long periods of time without re-circulating (Schenkel and Masopust, 2014; Shin and Iwasaki, 2013). To address whether virus-specific memory T cells in adipose tissue are contaminants from blood, we performed intravascular staining, in which fluorescent antibodies against CD4 or CD8 are injected intravenously moments before tissue harvest (Anderson et al., 2014); this technique identifies vascular T cells, including those in capillaries, from tissue-embedded T cells. To facilitate this analysis, we adoptively transferred congenic virus-specific TCR-transgenic P14+ CD8+ T cells (specific for $GP_{33–41}$) or SMARTA+ CD4+ T cells (specific for GP61–80) to separate mice, immunized with LCMV-Armstrong, and then performed the intravascular staining at day 38, a memory time point. Gating on donor cells (Ly5a+), we observed that the vast majority of memory T cells found in our WAT cell preparation were not contaminants from circulation but located within the parenchyma of the tissue (Figures 3A and 3B). These data also show that TCR-transgenic T cells persist in WAT, similar to endogenous memory T cells.

Flow cytometry was used to quantify the surface expression of various activation and memory markers on the donor memory T cells, comparing those in WAT with those in the spleen of the same mice (Figure 3C). Like splenic memory CD8+ T cells, CD8+ T cells in the WAT were $CD44^{hi}CD62L^{lo}$ but also showed evidence of activation. CD8+ P14 cells in the WAT tended to express more CD69 and Ly6C than splenic P14 cells but were $KLRG1^{lo}$ and $CD127^{lo}$ and showed limited expression of CD103, unlike resident T cells in the lung, skin, or intestines. Adipose tissue memory CD8+ T cells expressed higher amounts of CD122, suggesting that the cells may favor IL-15 for homeo-static maintenance. Memory SMARTA CD4+ T cells in WAT were $CD44^{hi}CD62L^{lo}CD69^{lo}CD103^{lo}$, similar to their splenic counterparts. However, CD4+ T cells in adipose tissue expressed far higher levels of Ly6C and CD11a, suggesting recent activation, and higher levels of CD122, perhaps also reflecting preferential use of IL-15.

In separate cohorts of infected mice, endogenous tetramer+ T cells were identified at multiple times after infection (Figure S3A). As expected, most of these CD8+ tetramer+ T cells were $CD127^{lo}KLRG1^{+}$ (short-lived effector cells) at days 9–13 in both tissues. There was an equivalent percentage of $CD127^{hi}KLRG1^{lo}$ (memory-phenotype effector cells) in both tissues at this time. Splenic memory T cells transitioned to $CD127^{hi}KLRG1^{lo}$ during memory (days 30–45), whereas significantly fewer memory CD8+ T cells in adipose tissue were $CD127^{hi}KLRG1^{lo}$ (Figures S3B and S3C), and most cells were low for both molecules. CX3CR1 has been used to distinguish central memory T (Tcm), effector memory (Tem), and peripheral memory (Tpm) cells that can migrate through peripheral tissues and into circulation (Gerlach et al., 2016). CX3CR1 was highly induced on virus-specific CD8+ T cells in the spleen, though it tended to be expressed on $CD127^{lo}$ cells during memory (Figures S3B and S3C). Significantly fewer CD8+ T cells in adipose tissue expressed CX3CR1, and tetramer+ CD4+ T cells weakly expressed CX3CR1 in both tissues at all

times (Figures S3D and S3E). There were significantly higher frequencies of adipose tissue CD4+ T cells that expressed Ly6C (Figures S3D–S3F), an activation marker associated with splenic Th1 cells with limited proliferative recall responses (Marshall et al., 2011). Overall, endogenous tetramer+ T cells in adipose tissue and spleen show expression patterns that resemble P14 and SMARTA T cells analyzed in those tissues.

Memory P14+ or SMARTA+ T cells were isolated from the adipose tissue and spleen of the same recipient mice, FACS-sorted to high purity, and analyzed by RNA sequencing (RNA-seq) (Figure 3D; Table S1). A number of differentially expressed genes were observed when comparing T cells from WAT and spleen (Figure 3D; Tables S2 and S3). For CD8+ T cells, 456 genes were significantly changed (up or down) in expression when comparing WAT cells with splenic cells (Table S2). Far more differentially expressed transcripts were observed for CD4+ T cells (2,868 genes) (Table S3), possibly reflecting the heterogeneity of CD4+ T cell lineages. Despite these differences in gene expression, when responding to infection, WAT memory T cells accumulated in the spleen and adipose tissue and made cytokines as well as splenic memory T cells (Figure S2). Thus, although memory T cells in adipose tissue are clonally related to those in the spleen, WAT memory T cells are physically separate and abundant and show changes in gene and protein expression during homeostasis that suggest they are a unique subset. Moreover, WAT memory T cells are able to vigorously respond to infection.

Diet-Induced Obesity Increases Memory T Cell Number

Obesity is associated with altered immune defenses against infections. To understand the relationship between T cells, viral infection, and obesity, we infected lean or high-fat diet-induced obese mice with LCMV-Armstrong and quantified virus control and antiviral T cell responses at multiple times, including at day 90, when the mice fed a high-fat diet showed a significant increase in body weight and perigonadal adipose weight (Figures 4A and 4B). Both obese and lean mice resolved the infection in the liver, lung, and kidneys within 1 week (data not shown).

Obese and lean mice generated similar numbers of $GP_{33–41}$-specific, $NP_{396–404}$-specific, $GP_{276–286}$-specific, and $NP_{205–212}$-specific CD8+ T cells and $GP_{61–80}$-specific CD4+ T cells at day 9, as measured by tetramer staining and ICCS of spleen cells (Figure 4C and data not shown). Interestingly, obese mice showed less T cell contraction at day 15 and maintained ~ 2- to 3-fold more virus-specific T cells to day 90 in the spleen (Figures 4C and 4D).

Obesity significantly increased the number of effector and memory T cells in adipose tissue (Figures 4C and 4D, bottom). At day 9, there were ~3-fold more $DbGP_{33}$+CD8+ T cells and 20-fold more $IAbGP_{67}$+CD4+ T cells in the adipose tissue of obese mice compared with lean mice (Figure 4C). The increase was sustained through day 90, when obese mice showed ~8-fold more memory CD8+ T cells and 5-fold more memory CD4+ T cells compared with lean mice. The adipose tissue of obese mice contained more memory T cells that could make IFNg (Figure 4D). The increase in adipose tissue memory T cells in obese mice was largely linked to the increase in adipose tissue mass in these mice (Figure 4E): when normalized, the number of virus-specific CD8+ T cells per gram adipose tissue was similar in mice fed control chow or high-fat chow. The density of virus-specific CD4+ T cells was increased at

days 8 and 15 by the high-fat diet, but the obesity-associated increase in memory CD4+ T cells correlated with WAT mass (Figure 4E). Obesity did not change the capacity of memory CD8+ T cells to make IFNg in the spleen or adipose tissue (Figure 4F); however, obesity altered memory CD4+ T cell expression of IFNg, slightly improving IFNg made by spleen cells and slightly decreasing IFNg made by WAT T cells (Figure 4F). In summary, obesity increases memory T cell number in the spleen and in adipose tissue in proportion to adipose tissue mass, without major changes to the ability of T cells to express the antiviral cytokine IFNg.

Immune Obese Mice Succumb to Re-challenge Infection

To understand the effects of obesity on memory cell responses and protection, we vaccinated lean or obese mice using LCMV-Armstrong, allowed the mice to establish a pool of memory cells, then re-challenged the mice with an aggressive variant that widely disseminates (LCMV-Clone13) (Figure 5A). Immune control of LCMV-Clone13 requires a vigorous memory T cell response and antibody, and immune mice typically control re-challenge infection in 5–7 days. Obesity increased T cell memory but did not affect serum levels of virus-specific IgG (Figure S4A). Although obesity was associated with impaired regulation of glucose levels (Figure S4B), this alteration was similar for both naive and LCMV-immune mice. Upon challenge infection, naive mice and lean immune mice showed modest weight loss and survived the infection (Figure 5B and data not shown). In contrast, immune obese mice showed greater loss of weight, and ~45% rapidly succumbed to infection. We observed that the blood and ascites of the immune obese mice showed greatly elevated lipase activity (Figure 5C), a sign of pancreatitis. We analyzed pancreases from naive and immune mice following the re-challenge infection (Figure 5D).

The pancreases of virus-challenged naive obese mice (second column) showed minimal to no detectable necrosis, and there was no apparent adipocyte necrosis, suggesting that the virus it self does not cause pancreatitis or fat necrosis. Re-challenged immune mice showed both significant influx of leukocytes into the pancreas and acinar cell damage (pale staining versus rich purple stain) compared with naive or unchallenged mice. Following infection, pancreatic damage was far more extensive in the obese mice but restricted to peripheral locations of the pancreas near adipose tissue rather than deeper within the pancreas (Figure 5D, right columns). Von Kossa staining revealed more calcium binding (gray) near the adipose tissue-pancreas boundary (Figure 5D, bottom row). Adipose tissue surrounding the pancreas showed more necrosis in the re-challenged obese immune mice than in the re-challenged lean immune mice or challenged naive mice (Figure 5D, middle row), and there was more calcium deposition onto perigonadal fat (not shown). Trichrome staining also revealed tissue damage at peripheral areas of the pancreas and in adipose tissue of re-challenged obese mice but not lean mice (Figure S3C). Re-challenged obese mice showed greatly increased levels of blood IL-6 (Figure 5E), consistent with pancreatitis (Park et al., 2015). TNF was undetectable in blood, but elevated the levels of IFNg suggest strong T cell activity in re-challenged obese mice.

Because virus-specific T cells are numerically increased in WAT and spleen during obesity (Figures 4C and 4D), we evaluated whether memory T cells contribute to pathogenesis.

Cohorts of LCMV-immune mice were depleted of CD4+ and CD8+ T cells across 2 weeks, which removed T cells systemically, including in adipose tissue (data not shown). T cell depletion prevented lipase release in the obese immune mice following challenge infection (Figure 6A), and there appeared to be less pancreatic necrosis and calcium deposition on adjacent adipose tissue (Figures 6B and S4C). Challenged obese mice showed a dramatic reduction in systemic calcium levels compared with challenged lean mice (Figure 6C), but T cell depletion prevented this loss. Re-challenged obese mice showed elevated levels of serum ALT, indicative of hepatocyte damage, which was prevented when T cells were depleted prior to re-infection (Figure 6D). Finally, obese immune mice rapidly developed hypothermia, which was prevented by T cell depletion (Figure 6E). Because all of these features of pathogenesis occurred only in obese LCMV-immune mice and were prevented by T cell depletion, we infer that memory T cell activity in mice with elevated levels of adipose tissue worsens health after re-challenge.

DISCUSSION

Obesity is increasingly prevalent throughout the world and is a significant health concern because it is associated with numerous immune-related disorders and susceptibility to infections. Here, we show that obesity predisposes mice to a unique form of pathogenesis during systemic viral infection. We demonstrate that LCMV infects adipose tissue and adipocytes. Virus-specific T cells accumulate in the WAT and are likely responsible for clearing infection there. The T cells in WAT then differentiate into memory T cells that appear phenotypically distinct from memory T cells in circulation or in lymphoid tissues. We also show that obesity increases the number of memory T cells systemically and in adipose tissue. Finally, we show that upon re-challenge, memory T cells respond to infection but cause a unique form of pathogenesis in obese mice that includes significant fat necrosis, systemic loss of calcium, multiple organ injury, and death.

The number of memory T cells in the adipose tissue of lean mice was surprisingly large. For perspective, the magnitude of the T cell response in the fat pads after LCMV is similar or greater than the total number of antigen-specific cells found in the spleens or lymph nodes of mice that have received protective T cell-inducing vaccines (e.g., DNA vaccine, peptide vaccine, recombinant Listeria monocytogenes). Adipose tissue is present throughout the body, so the total reservoir of memory T cells in adipose tissue in mice may be greater than what we have estimated. During obesity, primary T cells in adipose tissue were further increased, resulting in ~10^6 GP_{33}-specific CD8+ T cells at day 8, which is roughly one-third the number of found in the spleen; obesity increased the number GP_{61}-specific CD4+T cells in the fat pads to match the number found in the spleen. Obesity also increased the number of memory cells in adipose tissue, resulting in a population that is 10%–20% of the total number of memory T cells found in the spleen. Thus, although the spleen and lymph nodes are conventional places to track T cell responses and memory, our findings show that virus-specific T cells in WAT represent a major population of cells that have been neglected and are sensitive to the physiological changes caused by obesity.

Memory T cells in WAT appear to be unique, showing differences in RNA and protein expression compared with T cells in the spleen (Figures 3, S1F, and S3F). Recent analyses

of memory T cells in WAT have also identified differences in adipose Trm cells versus memory T cells in other peripheral tissues (Han et al., 2017). Likewise, we observe that virus-specific adi-pose T cells are $CD44^{hi}CD62L^{lo}$, a profile common to Tem and Trm cells but not Tcm. Roughly half of adipose tissue CD8+ T cells were CD69+ (often associated with Trm cells), as previously reported (Han et al., 2017), though virus-specific CD4+ T cells were uniformly CD69[C0]. WAT CD8+ T cells were mostly $KLRG1^{lo}$ but also under-expressed CD127, suggesting that they do not easily fit into the categories of short-lived effector cells or long-lived memory cells as defined for splenic CD8+ T cells, though the absence of KLRG1 is a characteristic of Trm cells in other peripheral tissues. WAT T cells showed relatively low expression of CD103 (Han et al., 2017), an integrin associated with Trm cells in epithelial sites (e.g., lung, skin, intestines), suggesting that T cells in WAT are also distinct from T cells in other non-lymphoid compartments. Memory T cells in adipose tissue showed increased expression of some chemokines (e.g., Cxcr4, Ccr2, Ccr9, Ccr2, Cxcr6) but under-expressed others (S1pr1, S1pr5, Ccr7, Cxcr5, Cx3cr1) compared with splenic memory T cells, suggesting that WAT T cells may be retained by distinct chemokine gradients, such as CXCL12 or CXCL16, which can be induced during viral infection. CX3CR1 expression levels have been used to distinguish Tcm ($CX3CR1^{lo}$), Tem ($CX3CR1^{hi}$), Tpm ($CX3CR1^{int}$), a subset that can recirculates through tissues, lymph, and blood, and Trm ($CX3CR1^{low/int}$), a non-migratory subset that populates peripheral tissues (Gerlach et al., 2016). Most memory CD8+ T cells in adipose were $KLRG1^{lo}$, $CD62L^{lo}$, $CX3CR1^{lo/-]}$, similar to Trm in other tissues (Herndler-Brandstetter et al., 2018). We could not discern a sizable $CX3CR1^{int}$ subset in WAT, suggesting that few of these cells are Tpm cells, and we have not examined their capacity to recirculate under homeostatic conditions. Adi-pose T cells expressed less CX3CR1 message, though we have not ruled out a role for CX3CL1-mediated endocytosis of CX3CR1 from the cell surface. Interestingly, WAT T cells expressed more Cd36 than splenic T cells, hinting that they may be specialized for fatty acid uptake and metabolism. Finally, early virus-specific memory T cells in adipose tissue show evidence of activation and undergo rapid cell division that is more extensive than the homeostatic cell division observed in lymphoid tissues, an observation consistent with *Yersinia pseudotuberculosis*-specific T cells in adipose tissue (Han et al., 2017). These findings suggest that there are local cytokines (adipokines) or residual antigens in adipose tissue that propagate cell division after infectious virus has been eliminated.

We show that obesity not only increases memory T cell number but converts a protective immune response to a lethal one. It may be that pathogenesis is exaggerated by alterations in glucose metabolism by memory T cells rather than changes to memory T cell abundance or location within adipose tissue. The increase in memory T cell number during obesity may be related to increases in leptin production, which can act on activated T cells that increase their expression of leptin receptor. Leptin signaling improves T cell proliferation and survival in culture (Papathanassoglou et al., 2006; Procaccini et al., 2017), and immune cell functions are reduced when there are deficiencies in leptin-receptor signaling (Moraes-Vieira et al., 2014; Procaccini et al., 2017). Obesity reduces the level of anti-inflammatory adiponectin (Barnes et al., 2015), possibly allowing pro-inflammatory signals to increase T cell frequencies. The outgrowth of memory T cells, including those in adipose tissue, may predispose to T cell-dependent pathogenesis during infection.

Adipose tissue can be targeted by LCMV, pichinde virus, HIV, SIV, adenovirus, vaccinia virus, and several species of parasites or bacteria (Chen et al., 2012; Couturier et al., 2015; Teixeira et al., 2016; Yang et al., 1985). T cells in adipose tissue can contribute to the control of acute infections (Figure 1; Chen et al., 2012; Han et al., 2017; Selin et al., 1998). However, under some circumstances, such as obesity (Figures 5 and 6) or heterologous viral infections (Chen et al., 2012; Selin et al., 1998; Welsh et al., 2010; Yang et al., 1985), T cells mediate pathogenesis. The divergent outcomes likely vary according to the number of memory T cells, as well as tropism and infection dose of the pathogen. Primary infection of mice with VV or LCMV fails to induce pathology in the WAT (Yang et al., 1985). However, mice that are hyper-immune to LCMV develop fat necrosis upon challenge with vaccinia viral infection, showing pathogenesis resembling the human syndromes, Weber-Christian disease and erythema nodosum (Welsh et al., 2010; Yang et al., 1985); although no pancreatic abnormalities were noted, roughly ~10% of the vaccinia virus-challenged mice succumbed (Yang et al., 1985). Heterologous infections that re-stimulate cross-reactive memory T cells can cause acute fat necrosis (Chen et al., 2012; Selin et al., 1998), a pathogenic outcome that may be greatly exacerbated in the context of obesity. Thus, extreme pathogenesis occurs when there is an excess of WAT and elevated frequencies of memory T cells.

The lethality seen in re-challenged obese mice was unusually rapid, occurring between days 2 and 4, suggesting that memory T cells acted quickly and did not require major proliferation to cause pathogenesis. We speculate that upon re-challenge, resident memory T cells respond to infected adipocytes or other adipose tissue-associated cells, killing infected cells and making IFNg and TNF. This may cause a massive release of lipid (triglycerides) that is processed to polyunsaturated fatty acids that exacerbate pancreatitis (Navina et al., 2011; Patel et al., 2015), ultimately leading to greater release of lipases and proteases by adjoining acinar cells (Figures 5 and 6). The pancreatic lipases may further contribute to adipocyte death, continuing the release of triglycerides and accumulation of polyunsaturated fatty acids that bind calcium (Dettelbach et al., 1990). The catastrophic loss of calcium (Figure 6C) may lead to systemic organ failure and death. Thus, we speculate that memory T cells directly kill infected adipocytes, leading to fat necrosis and hypocalcemia; pathogenesis is worse in obese mice, because obese mice have more adipose tissue memory T cells and more lipid in their adipocytes to sequester calcium. Nevertheless, the pancreas can be infected by LCMV, and we have not ruled out a role for virus-specific T cell activity within the pancreas in causing pathogenesis. Our histological evidence shows pancreatic damage along the border with WAT rather than uniformly across the pancreas, suggesting that the pathogenic process is related to WAT. Finally, we do not know whether T cell cytokines or cytolytic activity are essential for pathogenesis.

Pancreatitis is more frequent and severe in obese subjects compared with non-obese individuals (Huttunen and Syrjänen, 2013; Martínez et al., 2006). In view of our findings in mice, there should be analyses in humans to assess whether obesity increases the frequency or severity of enteric infections and whether T cells contribute to pancreatitis. Calcium supplementation has been used to treat patients with acute pancreatitis or sepsis (Ahmed et al., 2016), and it may be that replenishing calcium or inhibiting lipases (Patel et al., 2015) may avert lethal outcomes during viral infection in obese subjects.

Cumulatively, these data further implicate WAT as an important immunological organ (Grant and Dixit, 2015) with an abundant population of T cells that changes during obesity. Future analyses are needed to better understand how obesity-associated changes in adipose tissue-derived cytokines and inflammation alter memory T cell number and function and contribute to increased pathogenesis upon infection.

STAR★METHODS

CONTACT FOR REAGENT AND RESOURCE SHARING

Further information and requests for resources and reagents should be directed to the Lead Contact, Jason Whitmire (jwhitmir@email.unc.edu).

EXPERIMENTAL MODEL AND SUBJECT DETAILS

Mice—Male C57BL/6J mice were used in these studies. Male mice were used because they quickly gain weight when fed high fat diet. In some experiments, T cells were isolated from SMARTA TCR-transgenic (Tg+) mice or from P14 TCR Tg+ mice. The TCR Tg+ mice were crossed to B6.PL-*Thy1*^{a}/CyJ mice to generate TCR-Tg+/Thy1.1+ mice or to B6.SJLPtprc aPep3b/BoyJ to generate TCR-Tg+/ Ly5a+ mice. Adult male mice (8–10 weeks old) were infected by intraperitoneal injecton of 2×10^{5} plaque-forming units (PFU) LCMV-Armstrong strain. Other mice, including age-matched naive or LCMV-immune mice, were challenged with LCMV-Clone13 (2×10^{6} PFU, ip) at roughly 21–23 weeks of age and observed for up to 5 days for physical signs of illness. Animals were euthanized upon development of severe disease (eg, body temperature < 30˚C). All mouse experiments were approved by the University of North Carolina Hill Institutional Animal Care and Use Committee.

Virus—Plaque-purified LCMV was used to infect BHK-21 monolayers to prepare virus stocks. Virus stocks were mycoplasma free. Quantitation of infectious virus in the tissues was done by plaque assay on Vero cell monolayers.

Diet-induced obesity—Mice were fed high fat diet (60% of calories from fat) or control diet (10% of calories from fat) starting at 4–5 weeks of age. Mice were fed the same diet until they were sacrificed during experiments. Obese mice were > 40 g body weight and 12–15 weeks old when initially infected with LCMV-Armstrong.

T cell depletion—Mice were depleted of CD4+ and CD8+ T cells by 6 i.p. injections of 100 μg of anti-CD4 and anti-CD8 (or isotype controls) across 2 weeks (Nishimura et al., 2009).

Leukocyte isolation and purification—Single-cell suspensions were prepared from spleens, lymph nodes, blood, or perigonadal fat pads. Spleens and lymph nodes were physically disrupted over a 70 mm nylon cell strainer (Corning, NY). Erythrocytes were removed from spleen and bone marrow suspensions using ACK lysing buffer (Life Technologies-BRL, NY). Blood was spun over a histopaq cushion; leukocytes were isolated from the interphase. Fat pads were cut into small pieces, digested at 37˚C for 30 min with

1mg/ml collagenase (Calbiochem) and 10mg/ml DNase I (Sigma-Aldrich) in 10% RPMI before filtering through a 70 μm cell strainer. Leukocytes released from the fat pad were suspended in 44% Percoll, underlayed with 56% Percoll, and isolated from the interphase after centrifugation.

Adipocyte purification—Adipocytes were separated using a collagenase and differential centrifugation method (Deng et al., 2013; Grant et al., 2013). Perigonadal WAT (100mg from 3 mice) was minced, exposed to 1mg/ml collagenase, gently filtered through a 250 μm nylon mesh, and centrifuged for 10 minutes at 300 g. Three layers emerged with a low-density adipocyte layer on top, an aqueous layer of media, and a cell pellet. These 3 layers were collected separately, washed in media, and added to Vero cell monolayers in a plaque assay.

Cell culture—Vero cells and BHK cells were propagated in DMEM supplemented with 5% heat inactivated FBS, penicillin, streptomycin, and fungizone.

METHOD DETAILS

Flow cytometry—Single-cell leukocyte suspensions were prepared from the spleens and perigonadal WAT of male mice. Erythrocytes were removed from splenocyte preparations using ACK lysing buffer. The cells were washed and re-suspended in either 1% or 10% RPMI. The cells were stained directly *ex vivo* with combinations of fluorescently labeled mAbs or fluorescent-tetramers in the presence of unlabeled Abs against FcRs to block fluorochrome-conjugated Abs from binding to FcR+ cells. The intracellular cytokine staining (ICCS) assay was performed by culturing splenocytes with or without LCMV peptide in the presence of brefeldin A. After 5 hours of incubation, cells were stained for surface markers, washed, fixed with formaldehyde, and then permeabilized and exposed to mAbs specific for IFN- γ ,IL-2, and TNF. Antibody-stained cells were detected by FACSCalibur or LSRII cytometers (BD Biosciences), and the data were analyzed with FlowJo software (Tree Star).

Intravascular staining—This method distinguishes T cells that are located in the parenchyma of tissues from those in capillaries (Anderson et al., 2014). Mice were intravenously injected with PE-conjugated anti-CD4 or anti-CD80α to label T cells in circulation. Three minutes later, tissues were harvested and single cell suspensions were re-stained with FITC-conjugated anti-CD4 or anti-CD8 to identify to T cells within the tissue.

Cell proliferation assays—Intracellular staining for Ki67 was performed using a kit from BD Biosciences with anti-nuclear antigen (clone Ki-67). For the BrdU incorporation analyses, mice were given an initial intraperitoneal injection of 1 mg BrdU and fed 0.8 mg/ml BrdU in drinking water for 7 days. Incorporated BrdU in T cells was detected using an anti-BrdU flow kit from BD Biosciences, followed by flow cytometry analysis.

Antibody ELISA—Dilutions of sera from uninfected or virus-infected mice were assayed by ELISA using 96-well plates coated with virus-infected BHK cell lysate or uninfected BHK cell lysate. IgG bound to the plates was detected using HRP-conjugated anti-IgG.

RNA-sequencing—Virus-specific TCR-transgenic T cells were given to 10–20 mice followed by infection to generate memory cells. At day 50 post-infection, memory cells in the spleen or adipose tissue were identified by surface stained and FACS-sorted to ~98% purity by a FACSAria-II machine at the UNC FACS core. RNA was extracted from ~10^5 sorted cells (pooled from 5–10 mice each in 2 independent replicates; Table S1), and purified on oligo(dT) dynabeads for cDNA amplification. Adaptors were ligated and 100 bp reads were sequenced by the HiSeq 2000 Analyzer at the Scripps Microarray & NGS Core Sequencing Facility, La Jolla CA. The Genome Analyzer Pipeline Software (Casava v1.9) was used to perform the early data analysis, including base calling and demultiplexing of the barcodes. The reads in the fastq files were trimmed with the TruSeq adaptor and an additional 3bp on each end. The reads were then aligned to the mouse (mm9) genome using open source TopHat 2.0.9 and Bowtie2 programs. Reads were mapped to individual genes using HTSeq-count. EdgeR was used to identify significant differences between datasets (FDR < 0.05) and generate logCPM values that were used to generate scatterplots. Data were deposited in GEO under accession number GSE110212.

Histology & Immunofluorescence—Whole perigonadal adipose tissue samples were isolated in PBS, fixed in 10% buffered formalin overnight, and then stored in 100 proof EtOH. For some samples, 6 mm sections were cut and put onto slides and stained with hematoxylin and eosin (H&E) or Von Kossa stains. These samples were visualized through light microscopy with phase contrast on an Olympus BX61 microscope at the UNC Microscopy Services Laboratory. In other experiments, the perigonadal adipose tissue of male mice was whole-mount stained to visualize adipocyte lipid droplets ($BODIPY_{C12}$), nuclei (Hoechst), and CD3+ cells (clone-17A2) (Malide, 2008; Nishimura et al., 2009), followed by imaging analysis on a Zeiss-710 confocal laser-scanning microscope at the UNC Microscopy Services Laboratory. All histological processes were conducted by the Animal Histopathology Core Lab, Lineberger Comprehensive Cancer Center.

Lipase measurements—Lipase activity in peritoneal cavity and serum was determined Lipase Activity Colorimetric Assay Kit II (BioVision, Milpitas, CA). Peritoneal fluid was collected by introducing 2ml of sterile saline into the peritoneal cavity and then recovering the sample. The peritoneal fluid was clarified by centrifugation (5000 x g, 20 min) before the lipase assay.

Calcium measurements—Serum calcium concentrations were quantified by clinical chemistry tests at the UNC Animal Histopathology Core.

Alanine aminotransferase measurements—MaxDiscovery ALT Color Endpoint Assay was used to measure ALT activity in serum.

Glucose tolerance test—Mice were fasted for 16 hours and then injected with 1g/kg D-glucose ip. Blood was sampled from the tail vein at 15, 30, 60, and 120 minutes and with glucose concentrations determined by Bayer Contour Next glucometer.

QUANTIFICATION AND STATISTICAL ANALYSIS

Results are expressed as means ± SEM. Statistical analyses and graphing were done using Prism 6 software. Comparisons between groups were performed using unpaired two-tailed Student's t test or one-way analysis of variance (ANOVA) with Bonferroni multiple comparison test. Differences were considered significant when $p < 0.05$ (*); < 0.01 (**); < 0.001 (***). EdgeR was used to identify significant differences between datasets (FDR < 0.05) and generate logCPM values that were used to draw the scatterplots.

DATA AND SOFTWARE AVAILABILITY

The accession numbers for the RNA-seq data for the P14 and SMARTA T cells isolated from spleen or WAT are deposited in the GEO database under record number GSE110212.

Supplementary Material

Refer to Web version on PubMed Central for supplementary material.

ACKNOWLEDGMENTS

This work was partly supported by NIH grants R56AI110682, R21AI117575, and R01AI138337 to J.K.W. along with start-up funds from UNC-CH. Additional funds were made available through NIH-supported Nutrition Obesity Research Center (NORC) grant P30DK56350 to M.A.B. and a Pilot & Feasibility grant to J.K.W. J.S. and T.M. were supported by grant R01-GM10974. The flow cytometry core was supported in part by an NCI Cancer Center Core Support Grant (P30CA016086). The NIH Tetramer Core Facility provided tetramers.

REFERENCES

Ahmed A, Azim A, Gurjar M, and Baronia AK (2016). Hypocalcemia in acute pancreatitis revisited. Indian J. Crit. Care Med 20, 173–177. [PubMed: 27076730]

Anderson KG, Mayer-Barber K, Sung H, Beura L, James BR, Taylor JJ, Qunaj L, Griffith TS, Vezys V, Barber DL, and Masopust D (2014). Intravascular staining for discrimination of vascular and tissue leukocytes. Nat. Protoc 9, 209–222. [PubMed: 24385150]

Barnes MA, Carson MJ, and Nair MG (2015). Non-traditional cytokines: How catecholamines and adipokines influence macrophages in immunity, metabolism and the central nervous system. Cytokine 72, 210–219. [PubMed: 25703786]

Chen AT, Cornberg M, Gras S, Guillonneau C, Rossjohn J, Trees A, Emonet S, de la Torre JC, Welsh RM, and Selin LK (2012). Loss of anti-viral immunity by infection with a virus encoding a cross-reactive pathogenic epitope. PLoS Pathog 8, e1002633. [PubMed: 22536152]

Cinti S, Mitchell G, Barbatelli G, Murano I, Ceresi E, Faloia E, Wang S, Fortier M, Greenberg AS, and Obin MS (2005). Adipocyte death defines macrophage localization and function in adipose tissue of obese mice and humans. J. Lipid Res 46, 2347–2355. [PubMed: 16150820]

Couturier J, Suliburk JW, Brown JM, Luke DJ, Agarwal N, Yu X, Nguyen C, Iyer D, Kozinetz CA, Overbeek PA, et al. (2015). Human adipose tissue as a reservoir for memory CD4+ T cells and HIV. AIDS 29, 667–674. [PubMed: 25849830]

Deng T, Lyon CJ, Minze LJ, Lin J, Zou J, Liu JZ, Ren Y, Yin Z, Hamilton DJ, Reardon PR, et al. (2013). Class II major histocompatibility complex plays an essential role in obesity-induced adipose inflammation. Cell Metab 17, 411–422. [PubMed: 23473035]

Dettelbach MA, Deftos LJ, and Stewart AF (1990). Intraperitoneal free fatty acids induce severe hypocalcemia in rats: a model for the hypocalcemia of pancreatitis. J. Bone Miner. Res 5, 1249–1255. [PubMed: 2075838]

Díaz E, Rodríguez A, Martin-Loeches I, Lorente L, Del Mar Martín M, Pozo JC, Montejo JC, Estella A, Arenzana Á, and Rello J; H1N1 SEMICYUC Working Group (2011). Impact of obesity in patients infected with 2009 influenza A(H1N1). Chest 139, 382–386. [PubMed: 20688928]

Gerlach C, Moseman EA, Loughhead SM, Alvarez D, Zwijnenburg AJ, Waanders L, Garg R, de la Torre JC, and von Andrian UH (2016). The chemokine receptor CX3CR1 defines three antigen-experienced CD8 T cell subsets with distinct roles in immune surveillance and homeostasis. Immunity 45, 1270–1284. [PubMed: 27939671]

Grant RW, and Dixit VD (2015). Adipose tissue as an immunological organ. Obesity (Silver Spring) 23, 512–518. [PubMed: 25612251]

Grant R, Youm YH, Ravussin A, and Dixit VD (2013). Quantification of adipose tissue leukocytosis in obesity. Methods Mol. Biol 1040, 195–209. [PubMed: 23852606]

Han SJ, Glatman Zaretsky A, Andrade-Oliveira V, Collins N, Dzutsev A, Shaik J, Morais da Fonseca D, Harrison OJ, Tamoutounour S, Byrd AL, et al. (2017). White adipose tissue is a reservoir for memory T cells and promotes protective memory responses to infection. Immunity 47, 1154–1168.e6. [PubMed: 29221731]

Herndler-Brandstetter D, Ishigame H, Shinnakasu R, Plajer V, Stecher C, Zhao J, Lietzenmayer M, Kroehling L, Takumi A, Kometani K, et al. (2018). KLRG1(+) effector CD8(+) T cells lose KLRG1, differentiate into all memory T cell lineages, and convey enhanced protective immunity. Immunity 48, 716–729.e8. [PubMed: 29625895]

Huh JY, Park YJ, Ham M, and Kim JB (2014). Crosstalk between adipocytes and immune cells in adipose tissue inflammation and metabolic dysregulation in obesity. Mol. Cells 37, 365–371. [PubMed: 24781408]

Huttunen R, and Syrjänen J (2013). Obesity and the risk and outcome of infection. Int. J. Obes 37, 333–340.

Karlsson EA, Sheridan PA, and Beck MA (2010). Diet-induced obesity impairs the T cell memory response to influenza virus infection. J. Immunol 184, 3127–3133. [PubMed: 20173021]

Malide D (2008). Application of immunocytochemistry and immunofluorescence techniques to adipose tissue and cell cultures. Methods Mol. Biol 456, 285–297. [PubMed: 18516569]

Marshall HD, Chandele A, Jung YW, Meng H, Poholek AC, Parish IA, Rutishauser R, Cui W, Kleinstein SH, Craft J, and Kaech SM (2011). Differential expression of Ly6C and T-bet distinguish effector and memory Th1 CD4(+) cell properties during viral infection. Immunity 35, 633–646. [PubMed: 22018471]

Martínez J, Johnson CD, Sánchez-Payá J, de Madaria E, Robles-Díaz G, and Pérez-Mateo M (2006). Obesity is a definitive risk factor of severity and mortality in acute pancreatitis: an updated meta-analysis. Pancreatology 6, 206–209. [PubMed: 16549939]

Masopust D, Murali-Krishna K, and Ahmed R (2007). Quantitating the magnitude of the lymphocytic choriomeningitis virus-specific CD8 T-cell response: it is even bigger than we thought. J. Virol 81, 2002–2011. [PubMed: 17151096]

Milner JJ, and Beck MA (2012). The impact of obesity on the immune response to infection. Proc. Nutr. Soc 71, 298–306. [PubMed: 22414338]

Moraes-Vieira PM, Larocca RA, Bassi EJ, Peron JP, Andrade-Oliveira V, Wasinski F, Araujo R, Thornley T, Quintana FJ, Basso AS, et al. (2014). Leptin deficiency impairs maturation of dendritic cells and enhances induction of regulatory T and Th17 cells. Eur. J. Immunol 44, 794–806. [PubMed: 24271843]

Navina S, Acharya C, DeLany JP, Orlichenko LS, Baty CJ, Shiva SS, Durgampudi C, Karlsson JM, Lee K, Bae KT, et al. (2011). Lipotoxicity causes multisystem organ failure and exacerbates acute pancreatitis in obesity. Sci. Transl. Med 3, 107ra110.

Nishimura S, Manabe I, Nagasaki M, Eto K, Yamashita H, Ohsugi M, Otsu M, Hara K, Ueki K, Sugiura S, et al. (2009). CD8+ effector T cells contribute to macrophage recruitment and adipose tissue inflammation in obesity. Nat. Med 15, 914–920. [PubMed: 19633658]

O'Brien KB, Vogel P, Duan S, Govorkova EA, Webby RJ, McCullers JA, and Schultz-Cherry S (2012). Impaired wound healing predisposes obese mice to severe influenza virus infection. J. Infect. Dis 205, 252–261. [PubMed: 22147799]

Papathanassoglou E, El-Haschimi K, Li XC, Matarese G, Strom T, and Mantzoros C (2006). Leptin receptor expression and signaling in lymphocytes: kinetics during lymphocyte activation, role in lymphocyte survival, and response to high fat diet in mice. J. Immunol 176, 7745–7752. [PubMed: 16751422]

Park J, Chang JH, Park SH, Lee HJ, Lim YS, Kim TH, Kim CW, and Han SW (2015). Interleukin-6 is associated with obesity, central fat distribution, and disease severity in patients with acute pancreatitis. Pancreatology 15, 59–63. [PubMed: 25434497]

Patel K, Trivedi RN, Durgampudi C, Noel P, Cline RA, DeLany JP, Navina S, and Singh VP (2015). Lipolysis of visceral adipocyte triglyceride by pancreatic lipases converts mild acute pancreatitis to severe pancreatitis independent of necrosis and inflammation. Am. J. Pathol 185, 808–819. [PubMed: 25579844]

Procaccini C, La Rocca C, Carbone F, De Rosa V, Galgani M, and Matarese G (2017). Leptin as immune mediator: Interaction between neuroendocrine and immune system. Dev. Comp. Immunol 66, 120–129. [PubMed: 27288847]

Rosen ED, and Spiegelman BM (2014). What we talk about when we talk about fat. Cell 156, 20–44. [PubMed: 24439368]

Schenkel JM, and Masopust D (2014). Tissue-resident memory T cells. Immunity 41, 886–897. [PubMed: 25526304]

Selin LK, Varga SM, Wong IC, and Welsh RM (1998). Protective heterologous antiviral immunity and enhanced immunopathogenesis mediated by memory T cell populations. J. Exp. Med 188, 1705–1715. [PubMed: 9802982]

Sheridan PA, Paich HA, Handy J, Karlsson EA, Hudgens MG, Sammon AB, Holland LA, Weir S, Noah TL, and Beck MA (2012). Obesity is associated with impaired immune response to influenza vaccination in humans. Int. J. Obes 36, 1072–1077.

Shin H, and Iwasaki A (2013). Tissue-resident memory T cells. Immunol. Rev 255, 165–181. [PubMed: 23947354]

Smith AG, Sheridan PA, Harp JB, and Beck MA (2007). Diet-induced obese mice have increased mortality and altered immune responses when infected with influenza virus. J. Nutr 137, 1236–1243. [PubMed: 17449587]

Teixeira L, Marques RM, Ferreirinha P, Bezerra F, Melo J, Moreira J, Pinto A, Correia A, Ferreira PG, and Vilanova M (2016). Enrichment of IFN-g producing cells in different murine adipose tissue depots upon infection with an apicomplexan parasite. Sci. Rep 6, 23475. [PubMed: 27001522]

Tsatsanis C, Margioris AN, and Kontoyiannis DP (2010). Association between H1N1 infection severity and obesity-adiponectin as a potential etiologic factor. J. Infect. Dis 202, 459–460. [PubMed: 20557238]

Twig G, Geva N, Levine H, Derazne E, Goldberger N, Haklai Z, Leiba A, and Kark JD (2018). Body mass index and infectious disease mortality in midlife in a cohort of 2.3 million adolescents. Int. J. Obes. (Lond.) 42, 801–807. [PubMed: 29081504]

Welsh RM, Che JW, Brehm MA, and Selin LK (2010). Heterologous immunity between viruses. Immunol. Rev 235, 244–266. [PubMed: 20536568]

Yang HY, Joris I, Majno G, and Welsh RM (1985). Necrosis of adipose tissue induced by sequential infections with unrelated viruses. Am. J. Pathol 120, 173–177. [PubMed: 4025507]

Highlights

- A large and unique subset of memory T cells is present in white adipose tissue
- Obesity greatly increases memory T cell frequencies in lymphoid and adipose tissue
- Obesity leads to an unusual form of T cell-mediated pathogenesis during infection

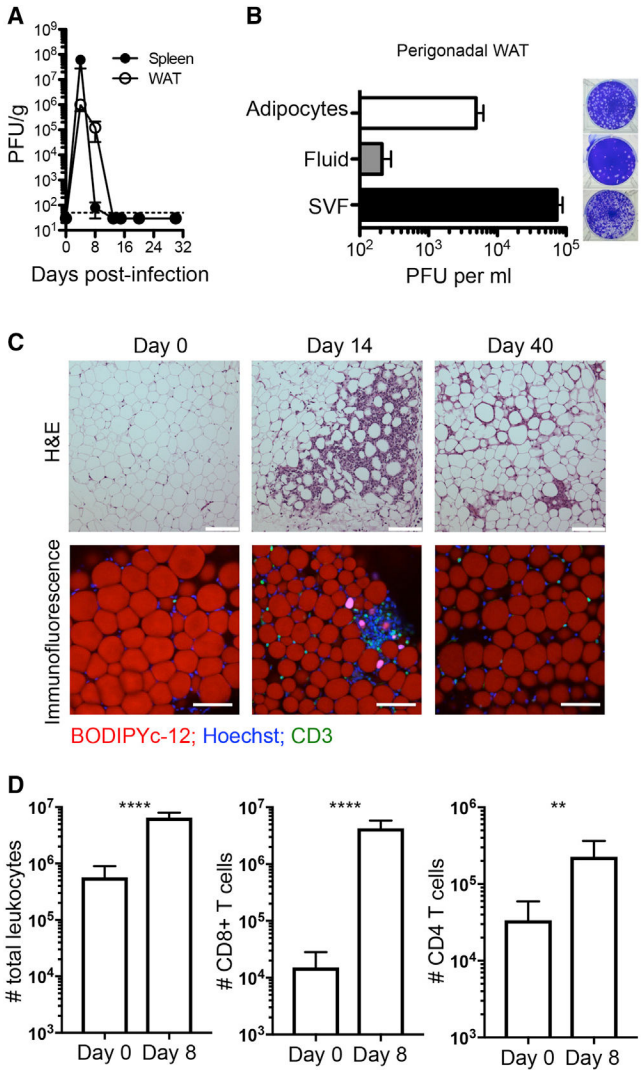

Figure 1. LCMV Infection of White Adipose Tissue

B6 mice were given LCMV-Armstrong (2 3 10^5 PFUs, intraperitoneal [i.p.]), and levels of virus in adipose and spleen and leukocyte abundance in adipose were determined.

(A) The line graphs represent virus levels mean (±SEM) in the spleen or perigonadal white adipose tissue (WAT) at the indicated days after infection. The dotted horizontal line indicates the limit of detection. Data are pooled from two experiments with three to six mice per group.

(B) Perigonadal fat pads were isolated from LCMV-infected mice at day 5 and assessed for viral infection. Gentle centrifugation was used to separate low density mature adipocytes from denser stromal vascular fraction (SVF) cell populations. The graph shows quantification of infectious virus (n = 3, one experiment), with an example of plaques developing in Vero cells.

(C) Perigonadal adipose tissue was harvested at the indicated days of infection and analyzed by microscopy. Top: representative sections stained with H&E; scale bar, 120 mm. Bottom: whole-mount staining reveals the lipid droplet in adipocytes ($BODIPY_{C12}$; red), cell nuclei

(Hoechst; blue), and infiltrating T cells (anti-CD3; green); scale bar, 100 mm. Data are representative of two experiments with two or three mice per group.
(D) Total number of leukocytes, CD8+ T cells, and CD4+ T cells recovered from fat pads before infection (n = 8) and at day 8 post-infection (n = 6). Data were analyzed using unpaired Student's t test with **$p < 0.01$ and ****$p < 0.0001$.

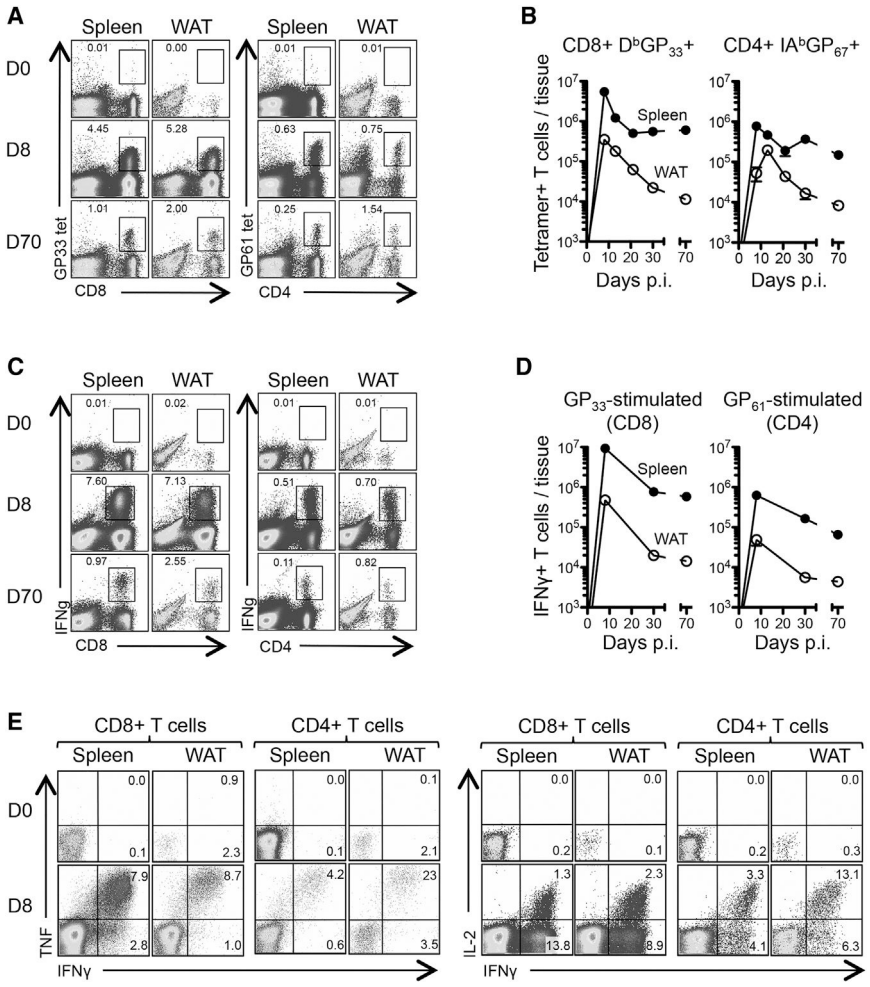

Figure 2. Virus-Specific T Cells Accumulate in WAT

Virus-specific T cells in adipose tissue and spleen were quantified at multiple times after acute infection by tetramer staining and ICCS.

(A) Representative dot plots identify DbGP$_{33}$+CD8+ T cells (left) and IAbGP$_{67}$+CD4+ T cells (right) before infection and at days 8 and 70 post infection. The numbers indicate the frequency of the tetramer+ cells among all live cells in the spleen or among leukocytes isolated from the fat pads.

(B) The number (mean ± SEM) of tetramer-positive T cells per spleen or fat pads at the indicated times post-infection. Data are drawn from two independent experiments with three to five mice per group.

(C) Representative dot plots show GP$_{33}$-specific CD8+ T cells or GP$_{61}$-specific CD4+ T cells expression of IFNg after peptide stimulation. The analyses are from the indicated days after infection, with numbers indicating the percentage of IFNg+ cells among all cells.

(D) The number (mean ± SEM) of IFNg+ epitopespecific T cells per tissue in spleen and fat pads as measured using ICCS assay at the indicated times post-infection. Data represent two experiments with five to nine mice per group.

(E) T cell co-expression of IFNg with TNF or IFNg with IL-2 in the spleen or fat pads at day 8. CD8+ T cells were stimulated with GP33–41 peptide;CD4+ T cells were stimulated with GP61–80 peptide.

See also Figure S1.

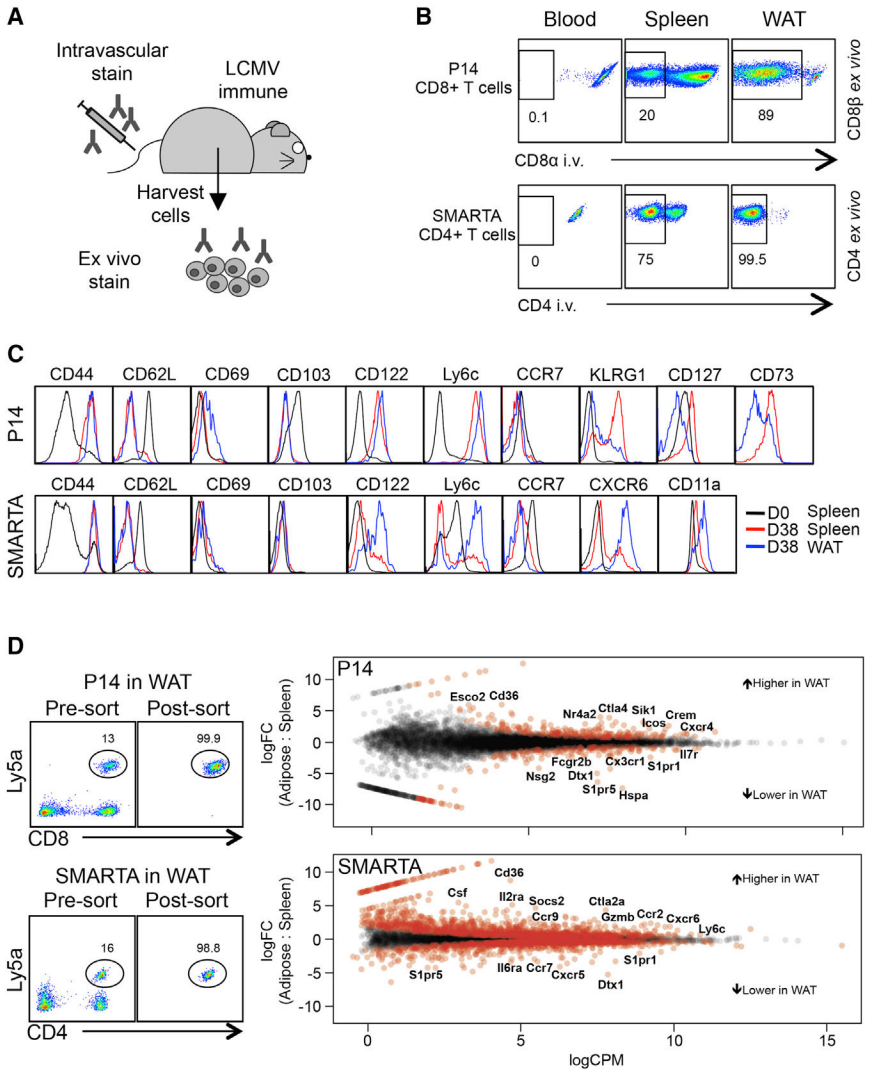

Figure 3. A Distinct Subset of Memory T Cells in WAT

(A and B) B6 recipient mice (Ly5a–) were given TCR-transgenic (Tg+) 2×10^4 P14 CD8+ (Ly5a+) T cells or SMARTA CD4+ (Ly5a+) T cells and then infected with LCMV-Armstrong 1–2 days later. At day 38 post-infection, intravascular (i.v.) staining was performed to label circulating donor CD4+ or CD8+ T cells and distinguish them from T cells within the spleen or adipose tissue.

(A) An illustration of the method whereby intravenous staining is coupled to *ex vivo* staining that labels all T cells in suspension.

(B) Representative dot plots showing the proportion of T cells protected from intravenous staining because of their location within the parenchyma of the spleen or WAT. Note that the vast majority of T cells purified from WAT are not contaminants from circulating subsets. Data represent three independent experiments with three or four mice per group. (C and D) B6 recipient mice (Ly5a–) were given TCR-transgenic (Tg+) splenic 2×10^4 P14 (Ly5a) or SMARTA (Ly5a+) T cells and then infected with LCMV-Arm 1–2 days after engraftment. At day 38, spleen and WAT cells were isolated and co-stained to identify the donor T cells and their expression of phenotypic markers.

(C) The histograms are gated on P14 memory cells (top) or SMARTA memory cells (bottom) and show their surface expression of the indicated molecules. Memory donor cells from spleen (red) or WAT (blue) are shown with naive splenic Tg+ cells (black). Data represent two experiments with four to six mice per group.

(D) Memory P14 and SMARTA donor cells from day 50 post-infection were FACS-purified from the spleen or adipose tissue and subjected to RNA sequencing to identify changes in gene expression. The dot plots show donor cells from adipose tissue before and after FACS. The graphs show EdgeR analysis of the RNA-seq data with log fold change (logFC) in RNA expression in WAT T cells relative to splenic T cells plotted against theamount of RNA per cell, expressed as log counts per million reads (logCPM). The red circles identify significant (false discovery rate [FDR] < 0.05) differences. These data are from two replicated experiments. Each replicate used pooled RNA isolated from ten (P14) or five (SMARTA) recipient mice.

See also Figures S2 and S3 and Tables S1, S2, and S3.

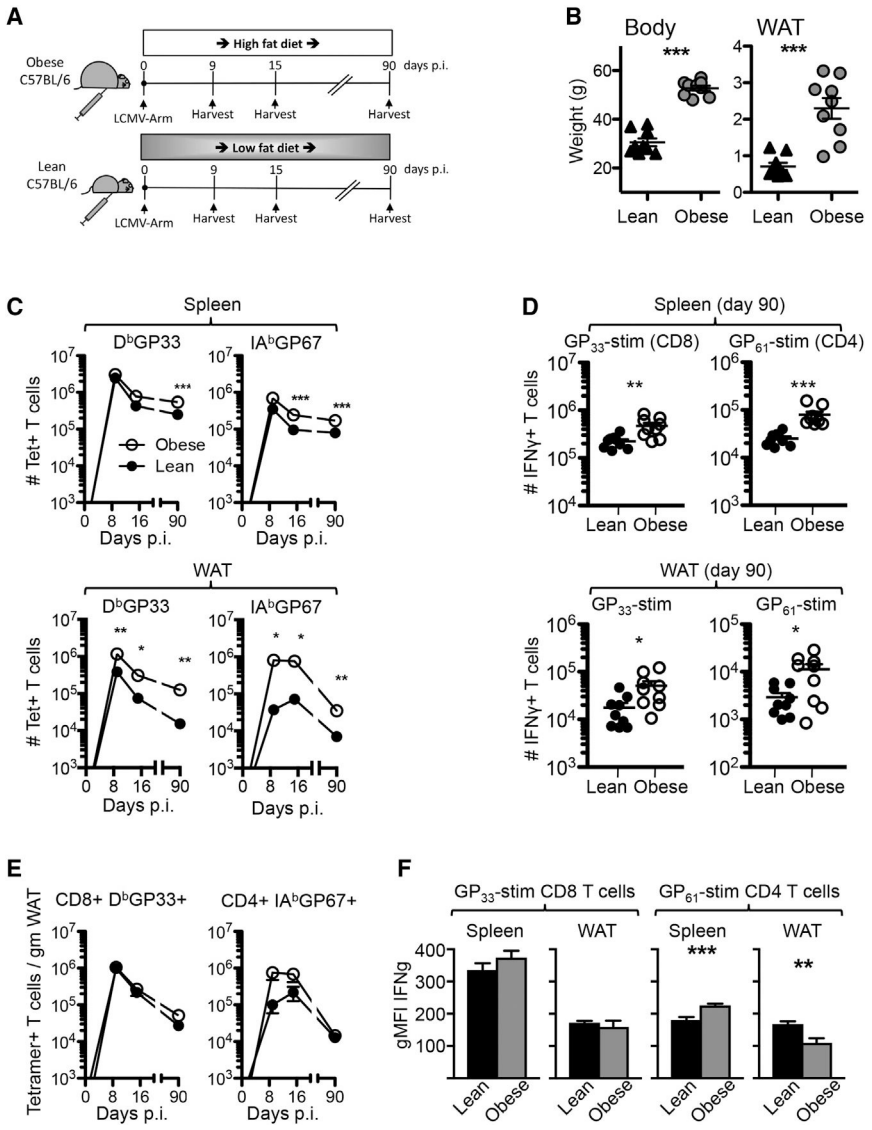

Figure 4. Diet-Induced Obesity Increases Memory T Cell Number

Mice were fed lean or high-fat diet for 8–9 weeks to establish obesity prior to LCMV-Armstrong infection. The number of virus-specific T cells in the spleen and fat pads was determined by tetramer staining and ICCS at multiple times after infection.

(A) An illustration of the experimental approach.

(B) The body weight of the mice and perigonadal fat pads at day 90 post-infection.

(C) The line graphs show the number (mean ± SEM) of tetramer-positive T cells per spleen (top) or WAT (bottom) at the indicated times post infection. Data are pooled from two to four independent experiments with a total of three to nine mice per group.

(D) The scatterplots show the number of GP_{33}-specific or GP_{61}-specific memory T cells that can make IFNg at day 90, as determined by ICCS assay. Each circle represents an individual mouse. Data represent four experiments with nine mice per group.

(E) The line graphs represent the number (mean ± SEM) of $DbGP_{33}$+CD8+ (left) or $IAbGP_{67}$+CD4+ (right) T cells per WAT divided by the weight of the fat pad. Data represent two or four experiments with three to nine mice per group.

(F) Lymphocytes were isolated from the spleen and fat pads of lean or obese mice at day 90 post infection and exposed to the indicated peptide in an ICCS assay. The graphs show the geometric mean fluorescence intensity (+SEM) among IFNg expression by T cells. Data represent four experiments with nine mice per group.

Significance determined by unpaired Student's t test: *$p < 0.05$, **$p < 0.01$, and ***$p < 0.001$.

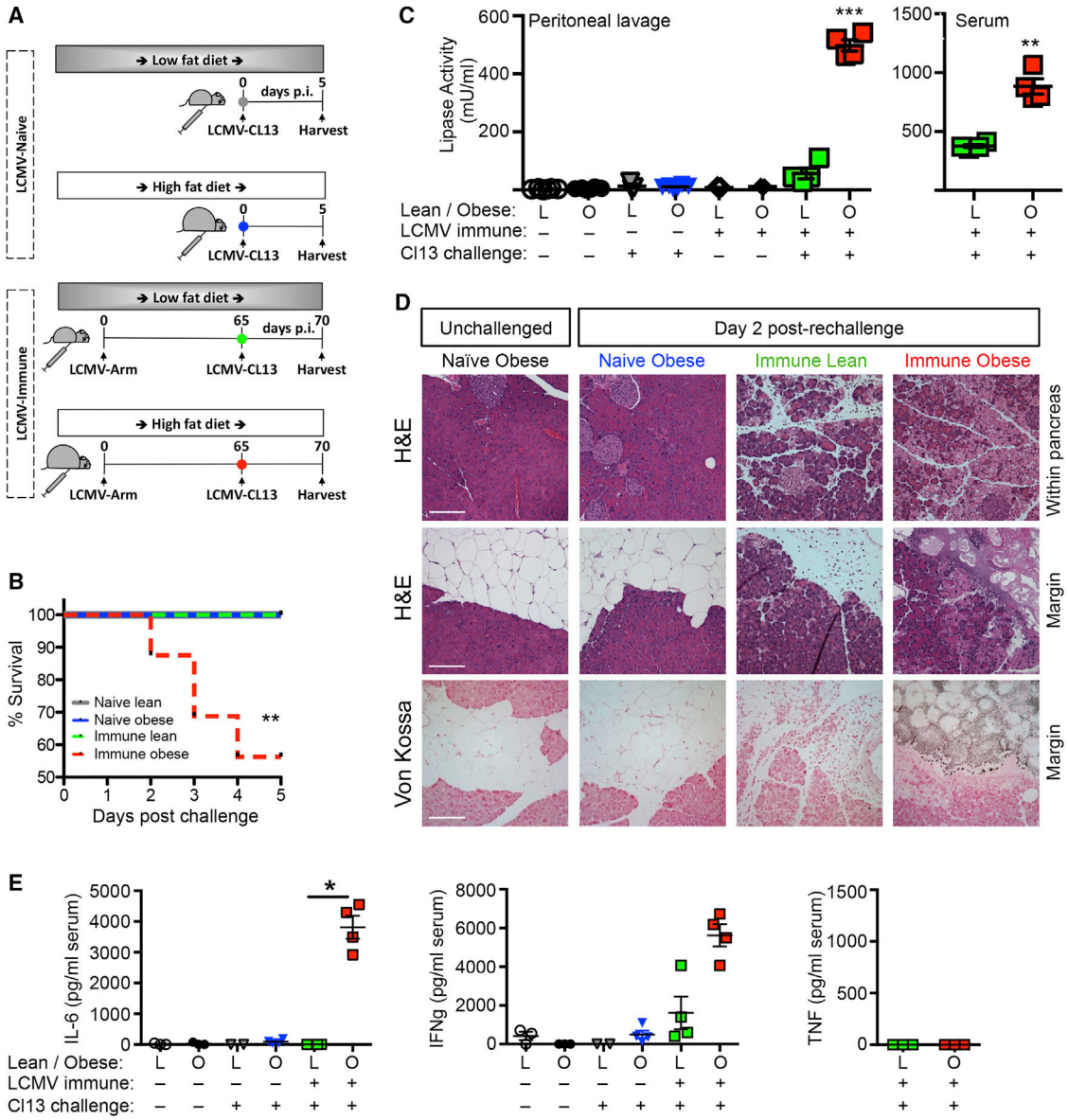

Figure 5. Immune Obese Mice Develop T Cell-Dependent Lethal Acute Pancreatitis upon Re-challenge

Cohorts of mice were fed lean or high-fat diet starting at 4–5 weeks of age until 13–15 weeks of age. Lean mice were <29 g (n = 10), and obese mice were >40 g (n = 13). Some of the mice were immunized with LCMV-Armstrong, and the rest were left LCMV naive. Sixty-five days later, the mice were challenged with LCMV-Clone13 (2×10^6 PFUs, i.p.) and analyzed 2 or 5 days later.

(A) An illustration of the experimental approach.

(B) Survival of naive (solid lines) and immune (dashed lines) mice after challenge, including mice requiring humane euthanasia. Among the re-challenged LCMV-immune mice, a Mantel-Cox log rank test revealed a significant difference (p = 0.0039) between the naive and obese mice. Data represent 7–16 mice/group.

(C) Lipase activity in ascites (left) and serum (right) at 2 days post-challenge infection. Dots on figure represent individual mice (3–6 per group, two independent experiments).
(D) Representative pancreas sections from the indicated four groups of mice at 2 days post-challenge infection. Sections were stained with H&E (upper two rows) or Von Kossa stain to reveal calcium deposition (dark gray, bottom row). The upper images show regions within the pancreas; the middle bottom images show the margin of the pancreas. Scale bar, 150 μm.
(E) Concentrations of IL-6, IFNg, and TNF in blood. Symbols represent individual mice (3 or 4 per group, two independent experiments). Significance determined by unpaired Student's t test: *$p < 0.05$, **$p < 0.01$, and ***$p < 0.001$.

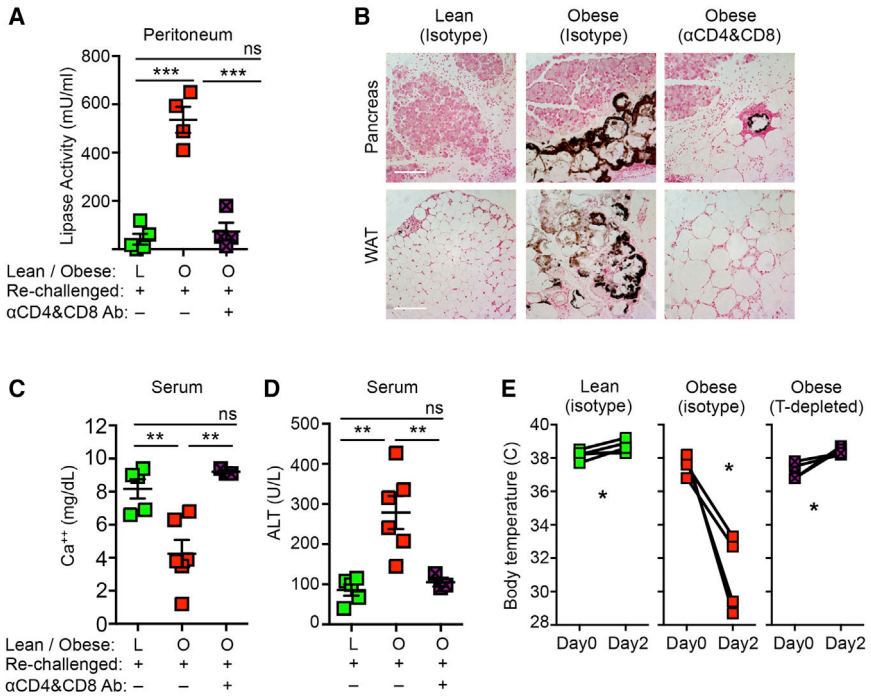

Figure 6. Memory T Cells Mediate Acute Pancreatitis and Adipose Tissue Necrosis

Cohorts of lean or obese immune mice were treated with antibodies to CD8 and CD4 to deplete T cells or treated with isotype control antibodies before challenge. Mice were analyzed 2 days after infection. Data compiled from two independent experiments with four to six mice per group.

(A) Lipase activity in the peritoneal cavity.

(B) Sections of pancreas and adipose stained with Von Kossa. Scale bar, 150 μm.

(C) Calcium concentrations in blood.

(D) ALT concentration in blood.

(E) Body temperature in individual mice. Significance determined by unpaired Student's t test: *$p < 0.05$, **$p < 0.01$, and ***$p < 0.001$.

(E) shows significance by paired Student's t test. See also Figure S4.

KEY RESOURCES TABLE

REAGENT or RESOURCE	SOURCE	IDENTIFIER
Antibodies		
TruStain fcX (anti-mouse CD16/32)	Biolegend	Cat#101320; RRID: AB_1574975
Anti-mouse CD3, BV421, clone 1452C11	Biolegend	Cat#100335; RRID: AB_10898314
Anti-mouse CD4, APC, clone RM45	Biolegend	Cat#100516; RRID: AB_312719
Anti-mouse CD4, PE, clone RM45	Biolegend	Cat#100511; RRID: AB_312714
Anti-mouse CD8α, APC, clone 536.7	Biolegend	Cat#100712; RRID: AB_312751
Anti-mouse CD80α, PE, clone 536.7	Biolegend	Cat#100707; RRID: AB_312746
Anti-mouse CD8β, FITC, clone YTS156.7.7	Biolegend	Cat#126605; RRID: AB_961293
Anti-mouse CD11a, FITC, clone M17/4	Biolegend	Cat#101106; RRID: AB_312779
Anti-mouse CD36, APC, clone HM36	Biolegend	Cat#102611; RRID: AB_571994
Anti-mouse CD44, FITC, clone IM7	Biolegend	Cat#103006; RRID: AB_312957
Anti-mouse CD44, Pacific Blue, clone IM7	Biolegend	Cat#103019; RRID: AB_493682
Anti-mouse CD62L, PE, clone MEL-14	Biolegend	Cat#104407; RRID: AB_313094
Anti-mouse CD69, PE, clone H1.2F3	Biolegend	Cat#104507; RRID: AB_313110
Anti-mouse CD69, BV605, clone H1.2F3	Biolegend	Cat#104529; RRID: AB_11203710
Anti-mouse CD103, AF488, clone 2E7	Biolegend	Cat#121407; RRID: AB_535949
Anti-mouse CD103, APC-Cy7, clone 2E7	Biolegend	Cat#121431; RRID: AB_2566551
Anti-mouse CD122, PE, clone 5H4	Biolegend	Cat#105905; RRID: AB_2125737
Anti-mouse CD127, APC, clone A7R34	Biolegend	Cat#135011; RRID: AB_1937217
Anti-mouse CD127, APC-Cy7, clone A7R34	Biolegend	Cat#135039; RRID: AB_2566160
Anti-mouse CCR7, PE, clone 4B12	Biolegend	Cat#120105; RRID: AB_389357
Anti-mouse CCR9, FITC, clone 9B1	Biolegend	Cat#129705; RRID: AB_1227482
Anti-mouse CXCR4, AF647, clone L276F12	Biolegend	Cat#146503; RRID: AB_2562590
Anti-mouse CXCR6, PE, clone SA051D1	Biolegend	Cat#151103; RRID: AB_2566545
Anti-mouse CX3CR1, PE, clone SA011F11	Biolegend	Cat#149005; RRID: AB_2564314
Anti-mouse KLRG1, PE, clone 2F1/ KLRG1	Biolegend	Cat#138407; RRID: AB_10574005
Anti-mouse KLRG1, BV605, 2F1/ KLRG1	Biolegend	Cat#138419; RRID: AB_2563357
Anti-mouse PD1, PE, clone 29F.1A12	Biolegend	Cat#135205; RRID: AB_1877232
Anti-mouse Ly5a, APC, clone A20	Biolegend	Cat#110713; RRID: AB_313502
Anti-mouse Ly6c, FITC, clone HK1.4	Biolegend	Cat#128005; RRID: AB_1186134
Anti-mouse Ly6c, BV605, clone HK1.4	Biolegend	Cat#128035; RRID: AB_2562352
Anti-mouse Thy1.1, OX-7, clone HIS51	Biolegend	Cat#202515; RRID: AB_961438
Anti-mouse Ki67, FITC, clone Ki-67	BD Biosciences	Cat#556026; RRID: AB_396302
Anti-BrdU, FITC, clone B44	BD Biosciences	Cat#347583; RRID: AB_400327

REAGENT or RESOURCE	SOURCE	IDENTIFIER
Anti-mouse IFN-γ, FITC, clone XMG1.2	Biolegend	Cat#505806; RRID: AB_315400
Anti-mouse TNF, APC, clone MP6-XT22	Biolegend	Cat#506308; RRID: AB_315429
Anti-mouse IL-2, APC, clone JES65H4	Biolegend	Cat#503810; RRID: AB_315304
Anti-mouse IgG-HRP	AbCam	Cat#Ab97023; RRID: AB_10679675
InVivoMAb anti-mouse CD8α, clone 2.43	BioXcell	Cat#BE0061; RRID: AB_1125541
InVivoMAb anti-mouse CD4, cloneGK1.5	BioXcell	Cat#BE00031; RRID: AB_1107636
InVivoMAb rat IgG2b isotype control	BioXcell	Cat#BE0090; RRID: AB_1107780
Bacterial and Virus Strains		
LCMV-Armstrong	Whitmire laboratory	N/A, generated in house
LCMV (Clone 13)	Whitmire laboratory	N/A, generated in house
Chemicals, Peptides, and Recombinant Proteins		
High-fat chow	Research Diets	D12492
Control chow	Research Diets	D12450B
Brefeldin A Solution (1,000X)	Biolegend	Cat#420601
Fixation Buffer	Biolegend	Cat#420801
Intracellular Permeabilization Buffer	Biolegend	Cat#421002
Biotinylated DbGP3341 monomer	NIH Tetramer core	N/A
Biotinylated DbNP396404 monomer	NIH Tetramer core	N/A
Biotinylated DbGP276286 monomer	NIH Tetramer core	N/A
APC-conjugated I-AbGP67 tetramer	NIH Tetramer core	N/A
Streptavidin-Allophycocyanin	Biolegend	Cat#405207
Heparin	Sanofi-Aventis	Lovenox
RPMI	Lonza	Cat#12167F
FBS	GIBCO	Cat#26140079
ACK lysing buffer	Life Technologies-BRL	Cat#A1049201
Collagenase, Type IV	Calbiochem	Cat#17104019
Percoll	GE Healthcare	Cat#17089102
DNase I	Sigma-Aldrich	Cat#D4527
ExoSAP-IT	Affymetrix	Cat#78200
$BODIPY_{C12}$	Invitrogen	D3835
Hoechst	Invitrogen	H1399
Critical Commercial Assays		
RNeasy Mini Kit	QIAGEN	Cat#74106
MaxDiscovery ALT Color Endpoint Assay	Bioo Scientific	Cat#346008
Lipase activity colorimetric assay kit II	BioVision	Cat#K722
Ghost Dye UV 450	Tonbobio	Cat#130868
ULtraComp eBeads	ThermoFisher Scientifc	Cat#01-2222-41
IL-6 ELISA MAX Standard Set	BioLegend	Cat#431301
IFN-γ ELISA MAX Standard Set	Biolegend	Cat#430801

REAGENT or RESOURCE	SOURCE	IDENTIFIER
TNF-alpha DuoSet ELISA	R&D SYSTEMS	DY41005
Deposited Data		
RNA seq: $CD8_+$ T cells; adipose	This paper	GEO Accession :GSE110212
RNA seq: CD8+ T cells; spleen	This paper	GEO Accession :GSE110212
RNA seq: CD4+ T cells; adipose	This paper	GEO Accession :GSE110212
RNA seq: CD4+ T cells; spleen	This paper	GEO Accession :GSE110212
Experimental Models: Cell Lines		
Vero-E6	Michael Buchmeier	The Scripps Research Institute, La Jolla, CA
BHK-21	American Type Culture Collection	Cat#CCL-10
Experimental Models: Organisms/Strains		
Mouse: C57BL/6J	Jackson Laboratory (purchased during last 7 years and bred at UNC)	Cat#000664
Mouse: B6.PL-*Thy1*^{a}/CyJ	Jackson Laboratory (purchased during last 7 years and bred at UNC)	Cat#000406
Mouse: B6.SJL-*Pfprc*^{a}*Pepc*^{b}/BoyJ	Jackson Laboratory (purchased during last 7 years and bred at UNC)	Cat#002014
Mouse: P14+ TCR-Tg (B6.Ly5a)	Backcrossed in Whitmire lab	N/A
Mouse: SMARTA+ TCR-Tg (B6.Ly5a)	Backcrossed in Whitmire lab	N/A
Software and Algorithms		
Flo-Jo Software (version 9.8.3)	Tree Star	https://www.flowjo.com
Prism 7	GraphPad	https://www.graphpad.com
Genome Analyzer Pipeline Software	Casava v1.9	https://www.illumina.com
TopHat 2.0.9	Johns Hopkins University	https://ccb.jhu.edu/software/tophat/index.shtml
Bowtie2	Johns Hopkins University	http://bowtie-bio.sourceforge.net/bowtie2/index.shtml
EdgeR	Walter and Eliza Hall Institute	http://www.bioconductor.org/packages/release/bioc/html/edgeR.html